Biochar X https://doi.org/10.48130/bchax-0026-0002

Original Research

Open Access

$Ca(OH)_2$-modified *Camellia oleifera* shell biochar: preparation, characterization, and adsorption of NH_4^+ and PO_4^{3-}

Min Chen[1#], Xichang Wu[1#], Yu Wang[1], Jie Wang[2*], Chaochan Li[1], Tianhua Yu[1] and Anping Wang[1*]

Received: 4 December 2025

Revised: 27 December 2025

Accepted: 6 January 2026

Published online: 30 January 2026

Abstract

Excessive nitrogen and phosphorus in aquatic systems trigger eutrophication and environmental contamination. Herein, $Ca(OH)_2$-modified *Camellia oleifera* shell biochar was fabricated as an adsorbent for NH_4^+ and PO_4^{3-} removal, with the effects of contact time, temperature, initial concentration, and pH on adsorption performance investigated, and the mechanisms clarified via kinetic/isothermal models combined with FT-IR and XPS characterizations. Results showed that NH_4^+ and PO_4^{3-} adsorption both fit the pseudo-second-order kinetic model, indicating chemisorption dominance. NH_4^+ adsorption complied with both Langmuir and Freundlich models (monolayer-multilayer coexistence), while PO_4^{3-} adsorption followed only the Freundlich model (predominant multilayer adsorption). Acidic conditions and low temperatures favored PO_4^{3-} uptake, whereas alkaline conditions promoted NH_4^+ adsorption, with adsorption capacity showing a decrease-then-increase trend with temperature elevation. Notably, the modified biochar maintained favorable performance in complex swine wastewater. Mechanistically, NH_4^+ removal was dominated by ion exchange, while PO_4^{3-} removal relied on the synergy of ion exchange and precipitation, with precipitation as the primary pathway. This work provides a cost-effective strategy for nutrient removal from wastewater via agricultural waste valorization.

Keywords: *Camellia oleifera* shells, Modified biochar, NH_4^+, PO_4^{3-}, Adsorption mechanism

Highlights

- Functionalized biochar was prepared from agricultural waste *Camellia oleifera* shells via chemical modification and pyrolysis.
- The adsorption mechanisms and interaction patterns of NH_4^+ and PO_4^{3-} on calcium hydroxide-modified biochar were further elucidated.
- Utilizing *Camellia oleifera* shells to produce modified biochar for treating NH_4^+ and PO_4^{3-} in water bodies achieves secondary utilization of agroforestry waste and resolves the disposal challenge of *Camellia oleifera* shell residues.

# Authors contributed equally: Min Chen and Xichang Wu

* Correspondence: Jie Wang (xbmdwjie@163.com); Anping Wang (anping-wang@gznu.edu.cn)

Full list of author information is available at the end of the article.

https://doi.org/10.48130/bchax-0026-0002

Graphical abstract

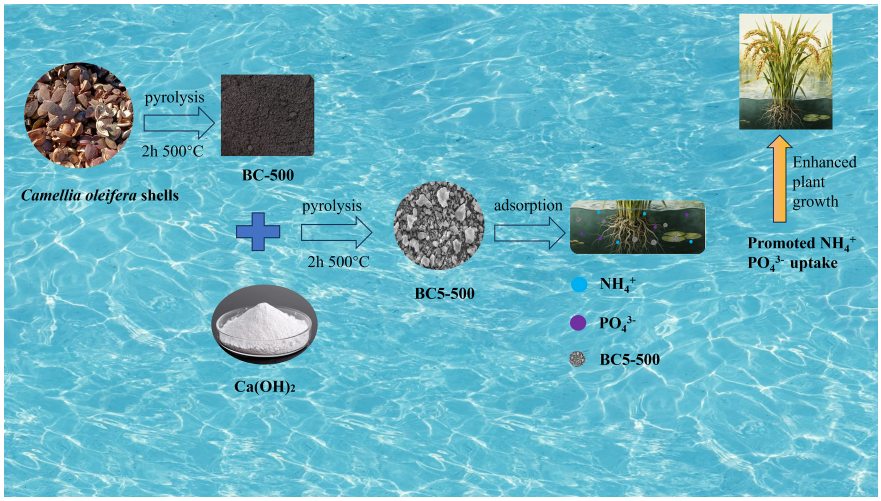

Introduction

As key plant-growth nutrients, nitrogen and phosphorus have fueled the widespread use of nitrogen- and phosphorus-based fertilizers. However, extensive human utilization and improper management have resulted in significant emissions of nitrogen and phosphorus ions (NH_4^+ and PO_4^{3-}) into the environment. Primary sources include agricultural activities and the discharge of domestic and industrial wastewater[1,2]. Excessive NH_4^+ and PO_4^{3-} in water bodies cause eutrophication, leading to environmental pollution. This disrupts the balance of nutrients in aquatic ecosystems, thereby damaging them[3–5]. Currently, there are multiple methods for removing NH_4^+ and PO_4^{3-} from water. Among such pollution control approaches, adsorption distinguishes itself as a widely adopted method due to its straightforward operation, quick process, and remarkable efficiency[3,6].

Derived from the anaerobic pyrolysis of biomass feedstocks, biochar is a solid carbonaceous material characterized by superior adsorption performance[7]. Its high porosity, ample specific surface area (SSA), good modifiability, as well as chemical attributes like oxygenated functional groups and unsaturated bonds, render it a widely used candidate for environmental pollutant abatement[8]. In biochar modification research, numerous scholars have employed diverse feedstocks and modification techniques to enhance its adsorption capacity for NH_4^+ and PO_4^{3-}. For example, Wang et al. prepared magnesium-loaded modified synthetic sludge-based biochar from anaerobic digestion sludge to remove PO_4^{3-} from aqueous solutions. Results demonstrated effective PO_4^{3-} removal under acidic conditions[9]. Jiang et al. prepared Mg-modified biochar from six different feedstocks for removing NH_4^+ and PO_4^{3-} from water. According to kinetics and thermodynamics research, cassava straw and banana straw biochar both exhibited high adsorption potential[10]. Li et al. prepared Fe-modified biochar using $FeCl_3$ as a modifier and applied it to adsorb NH_4^+ and PO_4^{3-}. This study involved multiple adsorption mechanisms[11]. In summary, existing studies indicate that through modification and composite techniques, the adsorption performance of biochar toward NH_4^+ and PO_4^{3-} has been effectively enhanced, with adsorption mechanisms gradually becoming clearer. However, biochar prepared from different raw materials and modification methods exhibits varying adsorption capacities for NH_4^+ and PO_4^{3-}. Compared to elements like Fe, Al, and Mg, calcium-based modified biochar, represented by calcium hydroxide, exhibits a strong affinity for NH_4^+ and PO_4^{3-}, significantly enhancing adsorption efficiency for these species[5,12–15]. Moreover, calcium is inexpensive, non-hazardous to ecosystems, and widely distributed in nature. Thus, calcium-modified biochar exhibits excellent environmental adaptability and safety, facilitating its long-term functionality in aquatic environments and making it an ideal metal element for biochar modification[16,17]. Moreover, biochar adsorbing PO_4^{3-} (primarily composed of $Ca_5(PO_4)_3(OH)$) is widely applied as a phosphorus fertilizer in soil[17,18]. Therefore, in this study, $Ca(OH)_2$ was selected as the modifier.

Camellia oleifera is a plant species belonging to *the genus Camellia* within the family *Theaceae*. The area used for *Camellia oleifera* production in China reached approximately 4.67 million hectares in 2023, projected to exceed 6 million hectares by 2025[19]. The processing of *Camellia oleifera* generates substantial shell waste that is difficult to manage, leading to resource wastage and environmental hazards. The rational utilization of discarded *Camellia oleifera* shells has become a critical issue for advancing the sustainable development of the *Camellia oleifera* sector[20]. However, *Camellia oleifera* shells possess high lignin and carbon content, making them an excellent raw material for producing carbon-based functional materials[21]. Therefore, this study utilizes *Camellia oleifera* shells as biomass feedstock to produce biochar, thereby unlocking new value for agricultural and forestry waste through circular utilization and writing a green chapter of 'turning waste into treasure'.

This study modified *Camellia oleifera* shell biochar using $Ca(OH)_2$ as a biochar modifier. It then adsorbed NH_4^+ and PO_4^{3-} in aqueous solutions, investigating the effects of time, initial concentration, solution pH, and reaction temperature on the adsorption of NH_4^+ and PO_4^{3-} by the modified biochar. Adsorption experiments were also conducted on NH_4^+ and PO_4^{3-} from actual swine wastewater. Finally, XPS and FT-IR characterizations were employed to elucidate the adsorption mechanisms of NH_4^+ and PO_4^{3-} by the modified biochar. This research elucidates the adsorption patterns, mechanisms, and environmental influences on NH_4^+ and PO_4^{3-} by biochar, aiming to offer experimental proof of the adsorption mechanisms of natural compounds comprising phosphorus and nitrogen. It also offers insights for managing organic pollutants in the environment, protecting resources, and promoting resource utilization.

Materials and methods

Reagents and materials

Potassium antimony tartrate (98%), ascorbic acid (99.99%), and calcium hydroxide (≥ 95%) were purchased from Shanghai Aladdin Biochemical Technology Co., Ltd. Potassium dihydrogen phosphate (99.5%), Ammonium molybdate (99.0%), Ammonium chloride (99.5%), and Dicyandiamide (AR) were purchased from Shanghai McLean Biochemical Technology Co., Ltd. *Camellia oleifera* shells were obtained from Tianzhu County, Guizhou Province, China.

Biochar and modified biochar preparation

The collected *Camellia oleifera* shells were repeatedly washed with deionized water to eliminate surface dust and soluble impurities. The cleaned material was then dried in an oven at 105 °C for 24 h to produce a constant weight. The dried shells were ground and sieved through a 40-mesh (aperture of approximately 0.45 mm) screen for further use.

A 10 g portion of the sieved *Camellia oleifera* shell powder was placed in a tube furnace. The sample was heated to 500 °C at a rate of 5 °C·min^{-1} under a nitrogen atmosphere and then pyrolyzed at that temperature for 2 h. The solid product was sieved through a 100-mesh screen (aperture of approximately 0.15 mm). The resulting material was labeled as BC-500 and collected for subsequent use.

Biochar derived from pyrolyzed *Camellia oleifera* shells was chemically modified using various reagents to produce a total of nine modified samples. For specific reagents and their quantities, please refer to the Supplementary Table S1. The general preparation procedure is described below. BC-500 and $Ca(OH)_2$ were mixed at a mass ratio of 1:2, followed by deionized water at a solid to fluid ratio of 1:10 g·mL^{-1}.The mixture was stirred for 24 h at 25 °C and 500 rpm, followed by vacuum filtration. The resulting solid was washed with deionized water and dried at 80 °C for 12 h.

The dried material underwent secondary pyrolysis in a tube furnace under conditions identical to those used for BC-500 preparation. The final $Ca(OH)_2$-modified biochar was designated as BC5-500.

Testing and characterization

The samples of biochar were described. Scanning electron microscopy (SEM, Apreo 2) was used to observe surface morphology. The specific surface area and pore structure were determined via N_2 adsorption-desorption analysis (TriStar II Plus 3030). Functional groups were identified by Fourier-transform infrared spectroscopy (FT-IR, Nicolet iS10) in the range of 4,000 to 400 cm^{-1}. The crystal structure was analyzed by X-ray diffraction (XRD, SmartLab 9), and the surface elemental composition was probed by X-ray photoelectron spectroscopy (XPS, Escalab 250Xi). The concentrations of NH_4^+ and PO_4^{3-} in solution were measured using a UV-vis spectrophotometer (UV-5500PC).

Adsorption experiments of biochar on NH_4^+ and PO_4^{3-}

Preliminary experiments were carried out to screen the most effective adsorbent for the removal of NH_4^+ and PO_4^{3-} from nine prepared biochar samples (Fig. 1). NH_4^+ and PO_4^{3-} stock solutions were prepared using NH_4Cl and KH_2PO_4, with initial concentrations of 100 and 600 mg·L^{-1}, respectively. The initial pH of each solution was adjusted to 10 for NH_4^+ and 6 for PO_4^{3-} using 0.1 mol·L^{-1} NaOH or HCl. For the adsorption experiments, 0.05 g of modified biochar was added to 30 mL of the corresponding solution and shaken at 150 rpm and 25 °C.

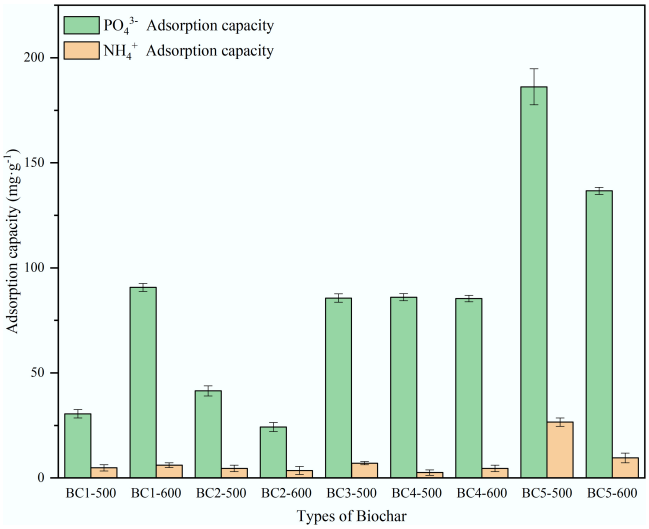

Fig. 1 Biochar screened for adsorption of NH_4^+ and PO_4^{3-}.

Table 1 Comparison among modified biochars for NH_4^+ and PO_4^{3-} adsorption

Biochar name	Adsorbate (mg·g^{-1})		Reaction kinetics	pH range	Ref.
	NH_4^+	PO_4^{3-}			
BS600	114.64	31.05	Pseudo-second-order kinetics	8.5–9.7	[22]
MgB	15.22	–	Pseudo-first-order kinetics	6.0–8.0	[23]
SB	> 28.2	> 120	Pseudo-second-order kinetics	Unadjusted pH	[24]
MgB-A	37.72	73.29	Pseudo-second-order kinetic	4.0–8.0	[25]

The adsorption time was set to 120 min for NH_4^+ and 360 min for PO_4^{3-}. After adsorption, the quantities of NH_4^+ and PO_4^{3-} were measured using UV-Vis spectrophotometry after the filtrate was separated using a 0.22 μm membrane filter. BC5-500 showed the highest adsorption capacity, reaching 26.66 mg·g^{-1} for NH_4^+ and 186.18 mg·g^{-1} for PO_4^{3-}. Its performance was further compared with that of modified biochars reported in other studies for NH_4^+ and PO_4^{3-} adsorption (Table 1). Given its considerable potential, BC5-500 was selected for subsequent systematic investigation.

Desorption experiment

To assess the reusability of BC5-500, cyclic adsorption-desorption experiments were performed. In each cycle, 0.10 g of BC5-500 was first subjected to adsorption under optimal conditions. Subsequently, the spent adsorbent was collected by filtration. The contaminant-laden BC5-500 was then subjected to static desorption in 50 mL of a 1.5 mol·L^{-1} NaOH solution at 25 °C for 2 h. After each desorption process, the material was filtered, cleaned with deionized water, and dried at 80 °C to prepare it for the subsequent cycle. Five successive cycles of this full adsorption-desorption process were carried out.

Data analysis

All experiments were performed in triplicate. Following the adsorption process, the solutions were filtered through a 0.45 μm membrane. The following equations were utilized to determine the adsorption capacity and removal efficiency based on the residual concentrations of NH_4^+ and PO_4^{3-}:

$$Qt = \frac{(C_0 - C) \times V}{m} \quad (1)$$

https://doi.org/10.48130/bchax-0026-0002

$$R = \frac{C_0 - C}{C_0} \times 100\% \quad (2)$$

In the equation, Qt denotes the adsorption capacity (mg·g^{-1}); R represents the removal efficiency (%); C_0 is the initial concentration of the adsorbate (mg·L^{-1}); C is the equilibrium or residual concentration after adsorption (mg·L^{-1}); V refers to the volume of the solution (L); and m is the mass of the adsorbent (g).

Results and discussion

Morphology and specific surface area measurements

Scanning electron microscopy (SEM) was employed to analyze the morphologies of BC-500 and BC5-500. The BC-500 surface appeared relatively smooth, with irregular lumpy particles adhering to it. These particles likely originated from mineral components that were incompletely carbonized (Fig. 2a, b). After modification via $Ca(OH)_2$ alkaline etching, the BC5-500 surface became rough, exhibiting a multilayered wrinkled structure (Fig. 2c, d). These wrinkles are expected to provide abundant reaction sites for subsequent adsorption processes.

The Brunauer-Emmett-Teller method was used to examine the pore structure of the materials. The nitrogen adsorption-desorption isotherms of both BC-500 and BC5-500 exhibit Type IV behavior and display H1 hysteresis loops, indicating that both materials possess mesoporous structures with relatively concentrated pore size distributions (Fig. 3). As evident from the pore size distribution diagram and Table 2 data, $Ca(OH)_2$ etching modification significantly increased the specific surface area of the biochar while introducing calcium active sites. This synergistic effect enhanced the adsorption capacity of BC5-500 for both NH_4^+ and PO_4^{3-}.

Evolution of functional groups upon biochar adsorption

FT-IR analysis of the material's chemical structure yielded the results shown in Fig. 4. The characteristic peaks at 3,427, 1,581, 1,387, and 1,265 cm^{-1} in the unmodified material BC-500 are attributed to

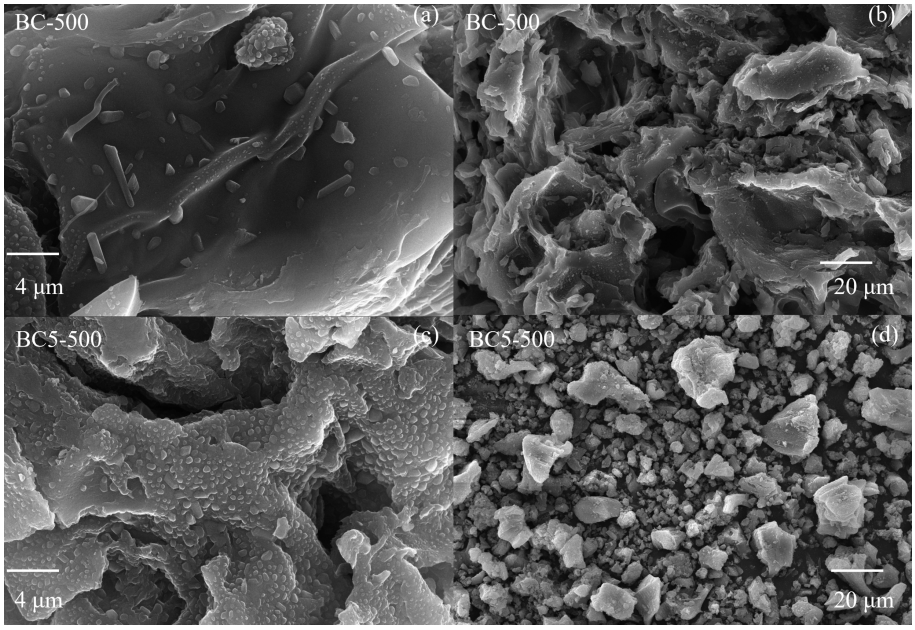

Fig. 2 SEM images of (**a**), (**b**) the biochar (BC-500), and (**c**), (**d**) the $Ca(OH)_2$-modified biochar (BC5-500).

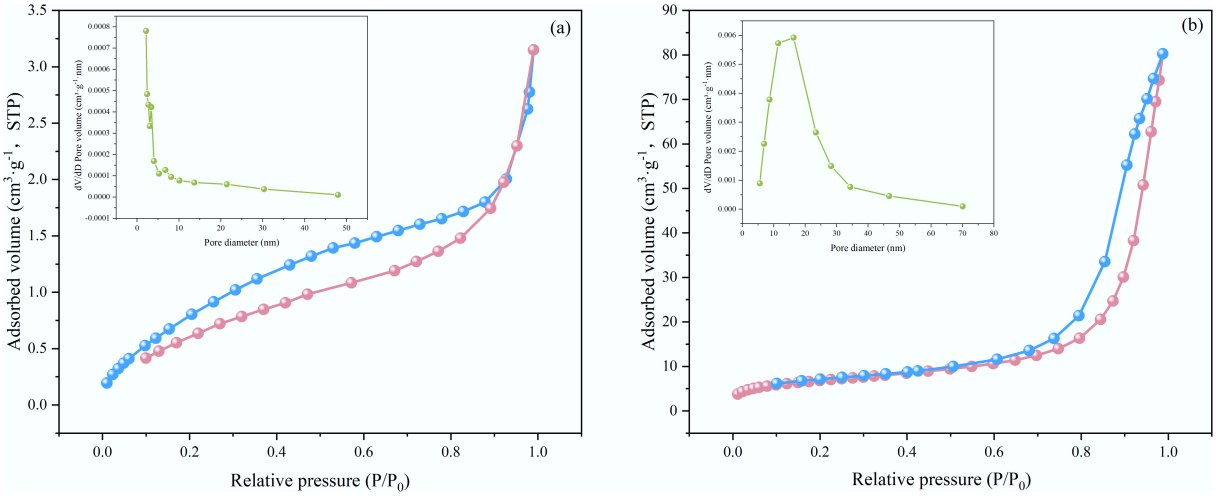

Fig. 3 Adsorption-desorption isotherms and pore size distribution of (**a**) BC-500, and (**b**) C5-500.

Table 2 Physical properties of BC-500 and BC5-500

Biochar name	S_{BET} ($m^2 \cdot g^{-1}$)	Total pore volume ($cm^3 \cdot g^{-1}$)	Average pore size (nm)
BC-500	3.71	0.0048	5.24
BC5-500	4.29	0.0079	20.01

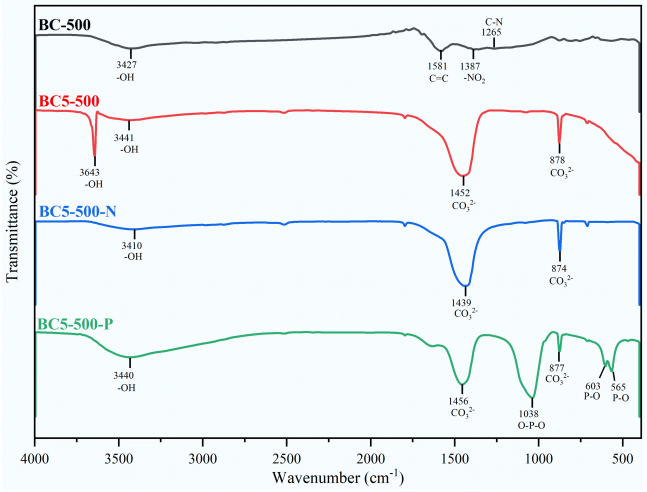

Fig. 4 FT-IR spectra of BC-500, BC5-500, and their derivatives after adsorption of NH_4^+ (BC5-500-N) and PO_4^{3-} (BC5-500-P).

functional groups (–OH, C=C, $–NO_2$, –C–N) in the pyrolysis residues of lignin and cellulose[6,26–31]. Following $Ca(OH)_2$ modification, the spectrum of BC5-500 exhibits significant changes. New absorption peaks appeared at approximately 878, 1,452, and 3,643 cm^{-1}, corresponding to Ca–O vibrations, asymmetric CO_3^{2-} stretching, and Ca-OH stretching, respectively. This indicates that calcium species were converted to CaO and partially carbonated to $CaCO_3$ during pyrolysis, while residual or hydrated hydroxyl groups remained on the surface[6,26–32]. These results confirm the successful loading of $Ca(OH)_2$ onto the biochar surface. Following NH_4^+ adsorption, the –OH vibration peak of water in the BC5-500-N spectrum was significantly weakened or disappeared, likely due to hydrogen bonding or ionic-dipolar interactions between oxygen-containing functional groups and NH_4^+[6,26–32]. After PO_4^{3-} adsorption, the residual Ca–OH peak in the BC5-500-P spectrum disappeared, and new peaks appeared at 603, 565, and 1,038 cm^{-1}, attributed to the bending vibration (P–O) and symmetric stretching vibration (O-P-O) of PO_4^{3-}, respectively. This indicates that PO_4^{3-} undergoes surface coordination with calcium active sites or forms calcium phosphate precipitates[33]. This change further confirms that PO_4^{3-} adsorption by the modified biochar is dominated by chemisorption.

XRD analysis of biochar modification and adsorption

The crystalline structure of the material was analyzed via XRD. BC-500 exhibited broadened diffraction peaks at 2θ = 29.9°, corresponding to the amorphous carbon matrix formed after pyrolysis and any poorly crystalline mineral components potentially present within it (Fig. 5a)[16,34,35]. Following modification, several new diffraction peaks appeared in the BC5-500 spectrum. Upon comparison with standard patterns, the diffraction peaks at 2θ = 23.1°, 29.4°, 36.0°, 39.4°, 43.2°, 48.5°, and 57.4° match those of the $CaCO_3$ standard pattern (PDF#98-000-0141); while those at 2θ = 18.2°, 34.4°, 47.5°, 51.2°, and 54.8° matched the $Ca(OH)_2$ standard card (PDF#97-009-1882). These results confirm the successful incorporation of a composite calcium phase comprising $CaCO_3$ and $Ca(OH)_2$, whose structure provides alkaline sites and precipitation active centers for subsequent adsorption processes[36].

The XRD pattern of BC5-500-N simultaneously reveals both $CaCO_3$ and $Ca(OH)_2$ phases, with the diffraction peak intensity of $Ca(OH)_2$ significantly diminished. This may be attributed to the oxygen-containing functional groups on the BC5-500 surface chemically adsorbing NH_4^+ from the water (Fig. 5b). The XRD pattern of BC5-500-P exhibits a new phase, whose characteristic diffraction peaks at 2θ = 25.9° and 32.3° align with the standard pattern for hydroxyapatite ($Ca_5(PO_4)_3(OH)$) (PDF#97-008-1442), indicating that PO_4^{3-} and Ca^{2+} combine on the material surface to form amorphous calcium phosphate, which subsequently recrystallizes into the thermodynamically more stable hydroxyapatite at the alkaline interface (Fig. 5b)[16,34,37]. This process further confirms that the biochar within BC5-500 functions as a multifunctional carrier and reaction promoter. In summary, BC5-500 exhibits pronounced adsorption capacity for both NH_4^+ and PO_4^{3-}, with the adsorption process accompanied by the formation of novel compounds.

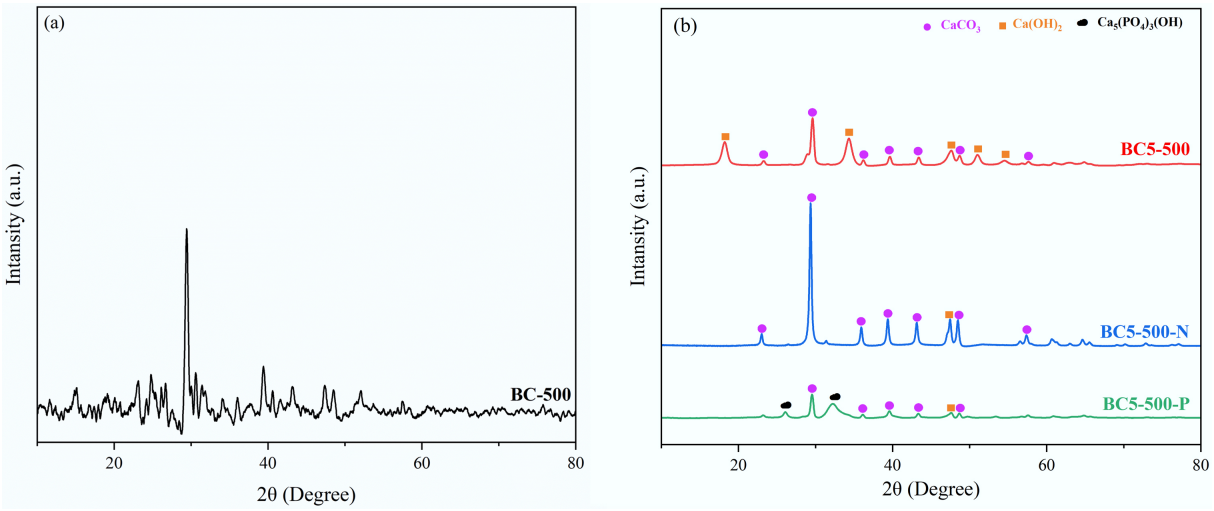

Fig. 5 XRD patterns of (**a**) BC-500, and (**b**) BC5-500 before and after adsorption (BC5-500, BC5-500-N, and BC5-500-P).

https://doi.org/10.48130/bchax-0026-0002

XPS analysis before and after biochar adsorption

To investigate structural changes in materials during PO_4^{3-} adsorption, XPS characterisation was performed on BC-500, BC5-500, BC5-500-N, and BC5-500-P.

XPS full-spectrum analysis indicates that C, N, O, and Ca elements were detected in all synthesised materials and their post-adsorption samples. Notably, a new characteristic P peak was only observed in the spectrum of BC5-500-P (Fig. 6a). This result directly confirms the successful synthesis of the adsorbent BC5-500 and indicates its adsorption capacity for NH_4^+ and PO_4^{3-}. Analysis of the C 1s spectrum for BC5-500-N in Fig. 6b reveals that, owing to incomplete pyrolysis, oxygen-containing functional groups and aromatic structures remain partially preserved within the biochar. Following NH_4^+ adsorption, the O–C=O and C=C contents in BC5-500-N decreased by 5.96% and 3.67%, respectively, while the C–O–C content increased by 9.6%. This shift likely arises from NH_4^+ adsorption, altering the local chemical environment of carbon. The O 1s spectra of BC5-500 and BC5-500-N (Fig. 6c) reveal reduced lattice oxygen content alongside the emergence of a peak at 532.6 eV, attributed to O–H/O–C[38,39]. The Ca 2p spectra for BC5-500 and BC5-500-N are shown in Fig. 6d. BC5-500 exhibits Ca-O-assigned peaks at 346.9 and 350.6 eV, indicating successful etching of $Ca(OH)_2$ onto the biochar surface, consistent with literature reports[40]. In BC5-500-N, the Ca 2p peak shifts blue overall and decreases in intensity due to interactions between oxygen-containing groups and NH_4^+. To better understand the adsorption procedure, N 1s spectra of BC5-500 and BC5-500-N were analysed (Fig. 6e). Peaks at 397.6, 398.7, and 401.2 eV in BC5-500 corresponded to intrinsic biochar nitrogen, N–(C=O)–N, and quaternary nitrogen structures, respectively[38–42]. Following NH_4^+ adsorption, BC5-500-N exhibits new peaks at 400.9, 402.5, 403.2, and 405.4 eV, which are attributed to graphitic nitrogen, C-NH_2^+, NH_4^+, and oxidised nitrogen species,

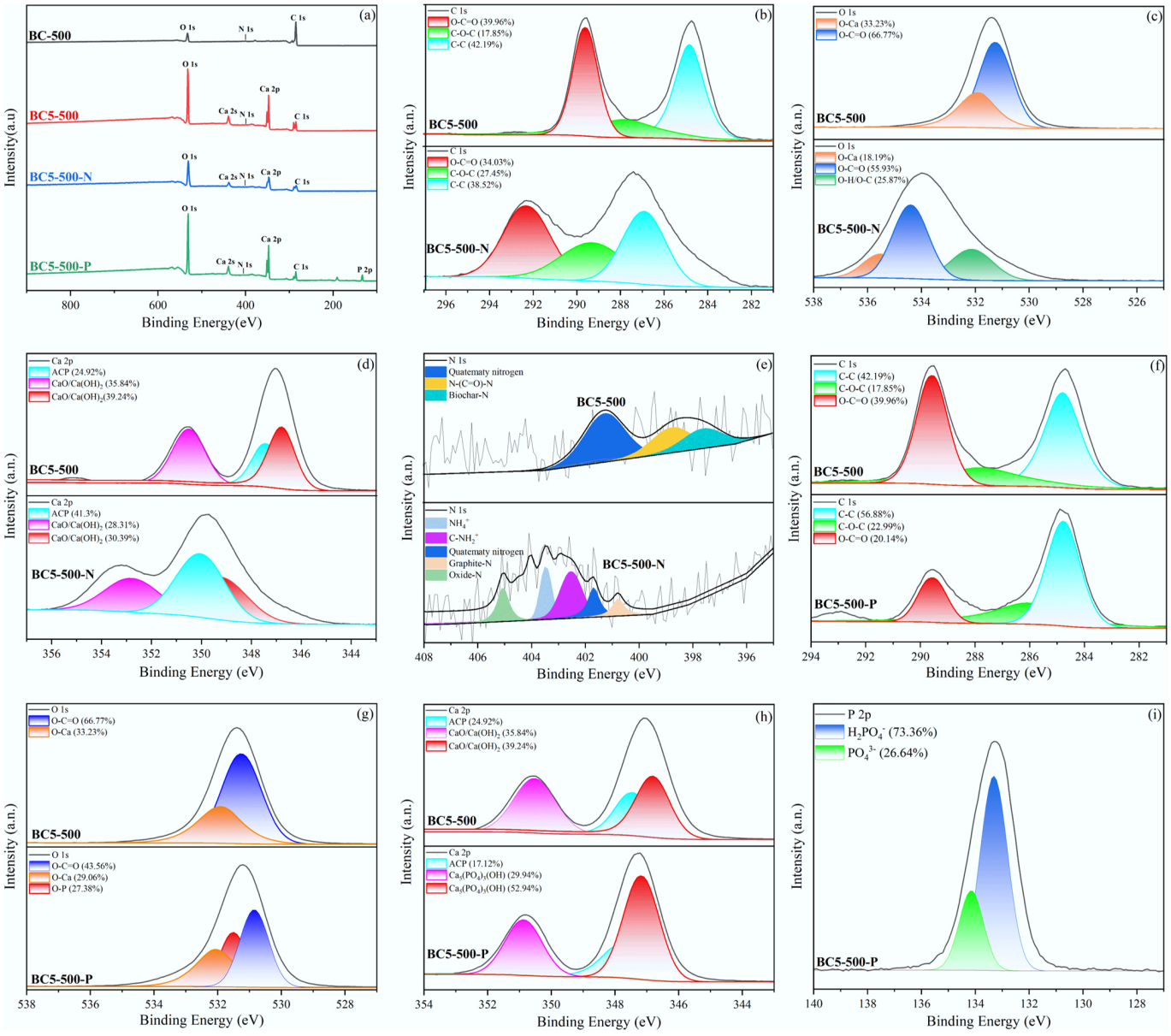

Fig. 6 XPS analysis of BC-500 and BC5-500 before and after adsorption: (**a**) survey spectra, (**b**)–(**e**) high-resolution C 1s, O 1s, Ca 2p, and N 1s spectra of BC5-500 and BC5-500-N, (**f**)–(**h**) high-resolution C 1s, O 1s, and Ca 2p spectra of BC5-500 and BC5-500-P, and (**i**) high-resolution P 2p spectrum of BC5-500-P.

respectively[38,41,42]. These results indicate that NH_4^+ adsorption on BC5-500 is mediated by Ca as the active centre, achieved through modulation of the local electronic structure.

Figure 6f compares the C 1s spectra of BC5-500 and BC5-500-P. A distinct redistribution of C–C, C–O–C, and O–C=O bond abundances occurred in BC5-500-P, driven by the formation of surface $Ca_3(PO_4)_2$. Concurrently, Fig. 6g reveals diminished intensities for the O–C=O and O–Ca peaks in the O 1s spectrum of BC5-500-P, potentially attributable to ion exchange between CO_3^{2-} and $H_2PO_4^-$/HPO_4^{2-}/PO_4^{3-}[31]. The Ca 2p spectrum of BC5-500-P (Fig. 6h) exhibits new Ca–O peaks at 347.5 and 351.0 eV, indicating that PO_4^{3-} is chemically bonded to the adsorbent surface. Figure 6i shows the P 2p spectrum of BC5-500-P, exhibiting characteristic double peaks at 133.5 eV (P $2p_{3/2}$) and 133.9 eV (P $2p_{1/2}$), with relative contributions of 73.36% and 26.64%, respectively. This further suggests that phosphate adsorption may involve a multi-step chemical reaction process.

Effect of solution pH

The pH of the solution is a key factor influencing the adsorption performance of biochar[43]. As shown in Fig. 7, the adsorption capacity first increases and then decreases with rising pH. It reaches its maximum at pH 11.0 (adsorption capacity of 15.44 mg·g^{-1} and removal rate of 25.73%), after which it decreases as pH continues to increase. Alkaline conditions favor the adsorption of NH_4^+. In an acidic environment, numerous H^+ battle with NH_4^+ for adsorption sites on the BC5-500 surface, therefore inhibiting adsorption[44]. For PO_4^{3-} adsorption, as pH increased, the adsorption capacity decreased. At pH 2.0, PO_4^{3-} adsorption is most effective, with an adsorption capacity of 172.04 mg·g^{-1} and a removal rate of 75.58%. This occurs because the form of phosphate present changes with pH: at pH < 2.1, it exists as H_3PO_4; at 2.1 < pH < 7.2, it primarily exists as $H_2PO_4^-$; at 7.2 < pH < 12.3, it mainly exists as HPO_4^{2-}; and at pH > 12.3, PO_4^{3-} becomes predominant[31]. In acidic conditions, Ca^{2+} on BC5-500 is more readily precipitated by binding with $H_2PO_4^-$. This process can be represented by the following equation:

$$Ca^{2+} + H_2PO_4^- + 2H_2O \rightarrow CaHPO_4 \times 2H_2O(s) + H^+ \quad (3)$$

However, in neutral and alkaline environments, the abundant OH^- in water competes with Ca^{2+} to preferentially form $Ca(OH)_2$ precipitates. Simultaneously, OH^- also competes with HPO_4^{2-} for adsorption sites, leading to a decrease in phosphorus adsorption capacity[44,45]. Within the experimental pH range, adsorption capacities consistently exceeded 150 mg·g^{-1}, with removal rates surpassing 55%. At pH 2.0 and 11.0, the maximum adsorption capacities for PO_4^{3-} and NH_4^+ were achieved, respectively. However, considering the pH conditions in real-world water environments and the need to obtain relatively high adsorption capacities, subsequent experiments for PO_4^{3-} and NH_4^+ were conducted at pH 6.0 and 10.0, respectively.

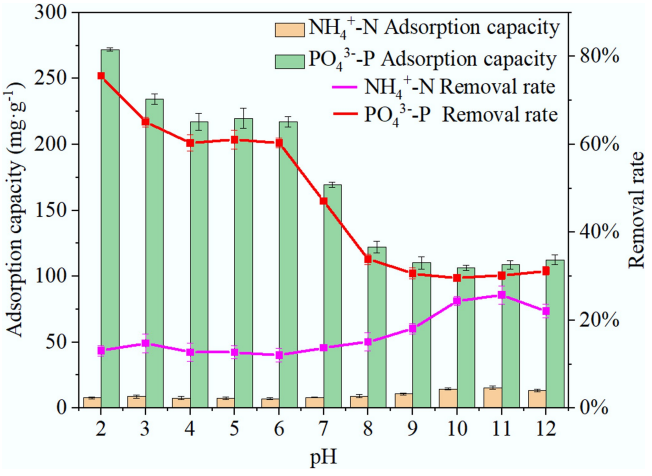

Fig. 7 Adsorption of NH_4^+ and PO_4^{3-} on BC5-500 as a function of solution pH.

Adsorption kinetics

The kinetic adsorption of PO_4^{3-} and NH_4^+ by modified biochar was modeled using pseudo-first-order and pseudo-second-order equations, respectively. Their expressions are shown in Eqs (4) and (5).

$$Q_t = Q_e\left(1 - e^{-k_1 t}\right) \quad (4)$$

$$\frac{t}{Q_t} = \frac{1}{k_2 \times Q_e^2} + \frac{t}{Q_e} \quad (5)$$

In the above equations, Q_e and Q_t represent the adsorption capacities at equilibrium (mg·g^{-1}), respectively; k_1 (min^{-1}) and k_2 (g·mg^{-1}·min^{-1}) denote the adsorption rate constants for pseudo-first-order and pseudo-second-order kinetics, respectively; t (min) is the adsorption time.

The kinetic adsorption profiles of NH_4^+ and PO_4^{3-} onto BC5-500 are presented in Fig. 8. The adsorption capacities for both pollutants increase rapidly in the initial stage, attaining equilibrium after approximately 60 and 90 min, respectively. This fast initial uptake rate can be attributed to the abundance of readily accessible active sites on the biochar surface. As adsorption progressed, the availability of these sites gradually decreased, resulting in a decreased adsorption rate until equilibrium was established.

As shown in Table 3, the pseudo-second-order kinetic model provides a substantially better fit than the pseudo-first-order model for both pollutants (R^2 > 0.986), and its calculated equilibrium adsorption capacities agreed closely with the experimental values. These results suggest that the adsorption process is likely governed by the number of surface active sites, indicating that chemical adsorption is a major factor[44,46].

Adsorption isotherms

The adsorption equilibrium data were analyzed using the Langmuir and the Freundlich isotherm models. The Langmuir model describes monolayer adsorption onto a homogeneous surface, while the Freundlich isotherm is an empirical model typically applied to characterize multilayer adsorption on heterogeneous surfaces. The corresponding fitted curves are presented in Fig. 9, with the mathematical expressions of the models given as follows:

$$Q_e = \frac{Q_m K_L C_e}{1 + K_L C_e} \quad (6)$$

$$Q_e = k_F C_e^{\frac{1}{n}} \quad (7)$$

Q_e (mg·g^{-1}) and Q_m (mg·g^{-1}) represent the equilibrium adsorption capacity and the theoretical saturation adsorption capacity of the Langmuir model, respectively; C_e denotes equilibrium concentration (mg·L^{-1}); K_L represents the Langmuir adsorption constant (L·mg^{-1}); $1/n$ is the Freundlich adsorption intensity coefficient; K_F((mg·g^{-1})·(mg·L^{-1})$^{-1/n}$) is the Freundlich adsorption constant.

The fitting parameters of the adsorption isotherm models are summarized in Table 4. For NH_4^+, both Langmuir and Freundlich models exhibit good agreement with the adsorption data (R^2 = 0.967 and 0.962, respectively), indicating that adsorption did not occur solely on an idealized homogeneous surface. The inherent heterogeneity of biochar, coupled with the contribution of multiple

https://doi.org/10.48130/bchax-0026-0002

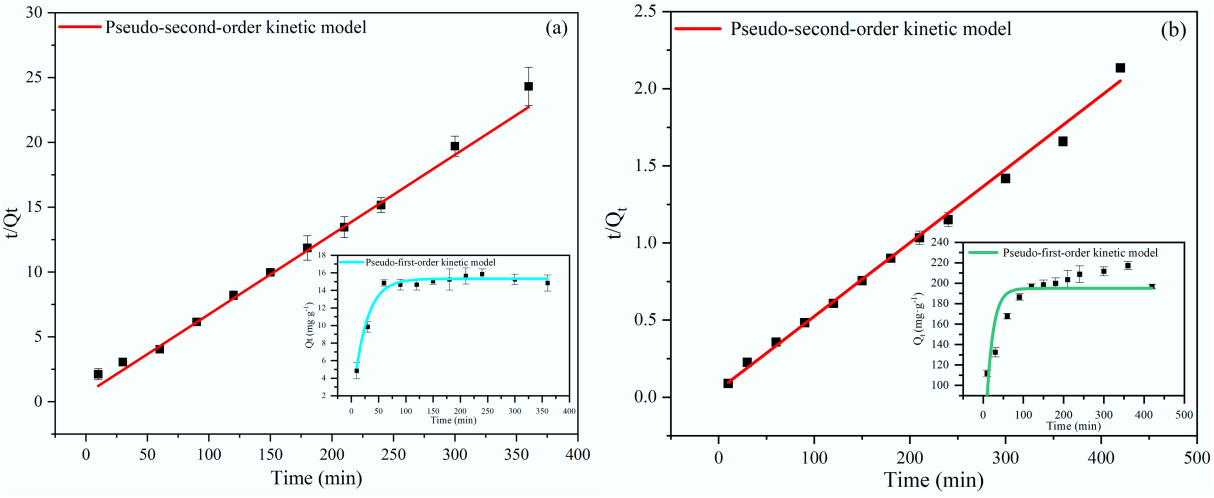

Fig. 8 (**a**) Adsorption kinetics of NH_4^+ on BC5-500. (**b**) Adsorption kinetics of PO_4^{3-} on BC5-500.

interactions such as ion exchange and surface complexation, likely governed the adsorption behavior. The dimensionless separation factor R_L derived from the Langmuir model was 0.64 ($0 < R_L < 1$), confirming the spontaneity and favorable nature of NH_4^+ adsorption under the experimental conditions[43].

For PO_4^{3-}, the adsorption data were better described by the Freundlich model (R^2 = 0.990), suggesting an energetically heterogeneous adsorption surface with potential multilayer characteristics. The Freundlich constant 1/*n* was 0.300 (< 0.5), indicating a very strong surface affinity of BC5-500 toward PO_4^{3-}[47]. This is primarily attributed to the Ca^{2+} introduced by the $Ca(OH)_2$ modification, which facilitates effective removal through the formation of insoluble calcium phosphate precipitates (Refer to the XPS characterization analysis). This chemical precipitation mechanism is substantially more dominant than conventional physical adsorption. Thermodynamically, the Freundlich parameter *n* exceeded 1 for both pollutants, confirming the excellent adsorption capacity of BC5-500 toward both NH_4^+ and PO_4^{3-}[48].

Table 3 Kinetic parameters for NH_4^+ and PO_4^{3-} adsorption onto BC5-500

Biochar name	Adsorbate	Pseudo-first-order kinetic model			Pseudo-second-order kinetic model		
		Q_e	K_1	R^2	Q_e	K_2	R^2
BC5-500	NH_4^+	15.33	0.04148	0.9371	16.27	0.00012	0.9863
	PO_4^{3-}	194.94	0.06142	0.7500	209.65	0.00047	0.9962

Effect of reaction temperature

There are two phases to the effect of temperature on NH_4^+ adsorption performance, as illustrated in Fig. 10. During the initial phase, at temperatures between 20–30 °C, the adsorption capacity and removal efficiency of BC5-500 for NH_4^+ decrease with increasing temperature, reducing by 4.6 mg·g^{-1} and 7.67%, respectively. In the second phase, at temperatures between 30 and 45 °C, the adsorption capacity for NH_4^+ increases with rising temperature. Overall, adsorption performance for NH_4^+ shows a pattern of declining and then rising. Regarding adsorption performance for PO_4^{3-}, both adsorption capacity and removal efficiency decreased with increasing temperature. Adsorption capacity dropped from 220.22 to 166.39 mg·g^{-1}, while removal efficiency decreased from 61.17% to 46.22%. This result suggests that elevated temperature significantly inhibits the adsorption process.

Relevant thermodynamic parameters for the adsorption process were calculated using the following equations[49]:

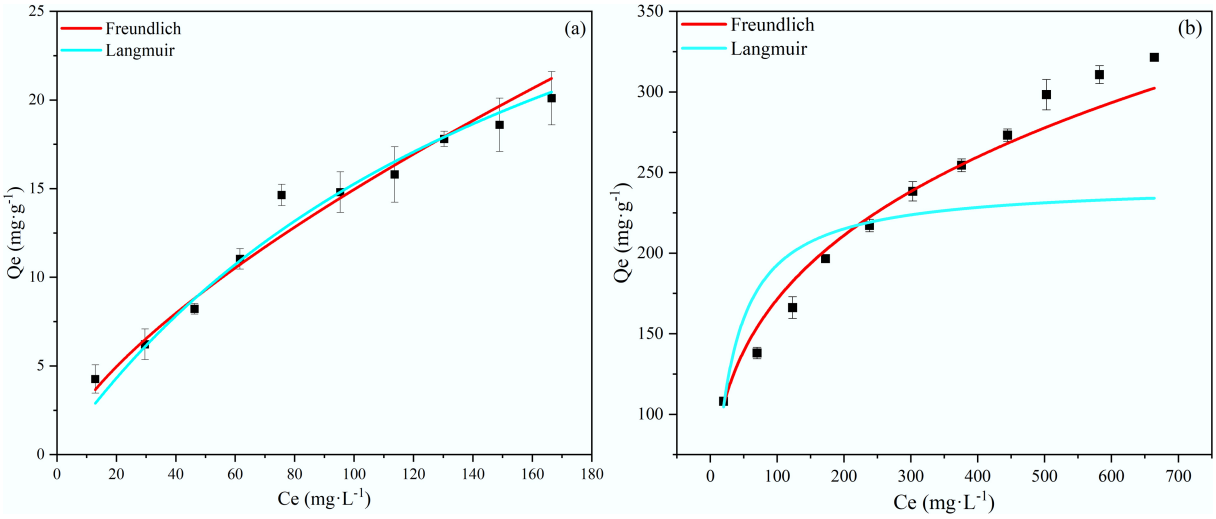

Fig. 9 Adsorption isotherms of (**a**) NH_4^+, and (**b**) PO_4^{3-} on BC5-500.

Table 4 Parameters of the adsorption isotherms for NH_4^+ and PO_4^{3-} onto BC5-500

Biochar name	Adsorbate	Langmuir			Freundlich			
		Q_m	K_L	R^2	n	K_F	R^2	$1/n$
BC5-500	NH_4^+	41.87	0.00574	0.967	1.145	0.632	0.962	0.873
	PO_4^{3-}	243.33	0.0380	0.868	3.335	43.077	0.990	0.300

$$\Delta G^o = -RT \ln k_0 \quad (8)$$

$$\Delta G^o = \Delta H^o - T\Delta S^o \quad (9)$$

$$\ln k_0 = \frac{\Delta S^o}{R} - \frac{\Delta H^o}{RT} \quad (10)$$

In the formula: ΔG^o (kJ mol^{-1}) is the standard Gibbs free energy; ΔH^o (kJ mol^{-1}) is the standard enthalpy change; ΔS^o (J·mol^{-1} K^{-1}) is the standard entropy change; R is the gas constant; k_0 is the adsorption equilibrium constant.

The thermodynamic parameters ($\Delta G°$, $\Delta H°$, and $\Delta S°$) for the adsorption process were determined at various temperatures and are presented in Table 5.

For NH_4^+ adsorption, as the temperature increased to 30–45 °C, $\Delta H° > 0$ and $\Delta S° > 0$, indicating a shift to an endothermic process with increasing entropy. Accordingly, the adsorption capacity rose with temperature, demonstrating a high-temperature-driven characteristic.

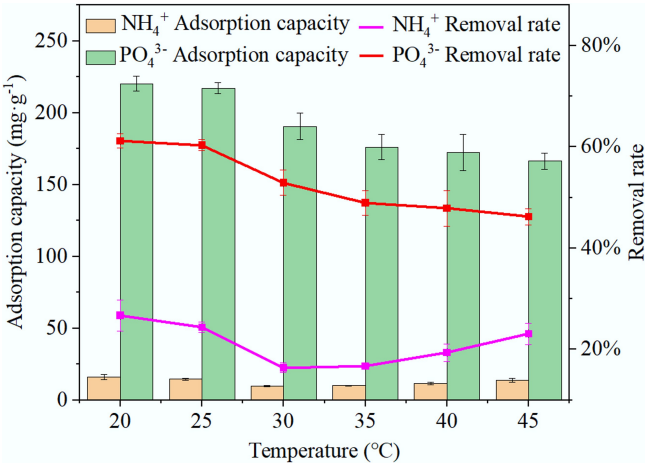

Fig. 10 Influence of reaction temperature on the adsorption capacity of BC5-500 for NH_4^+ and PO_4^{3-}.

Table 5 Thermodynamic parameters for the adsorption of NH_4^+ and PO_4^{3-} onto BC5-500

Biochar name	Adsorbate	Temperature (°C)	K_0	ΔG^0	ΔH^0	ΔS^0
BC5-500	NH_4^+	293	0.219	3.700	45.645	167.890
		298	0.195	4.067		
		303	0.118	5.390		
		308	0.121	5.417		
		313	0.144	5.036		
		318	0.180	4.535		
	PO_4^{3-}	293	0.945	0.1367	−20.896	−71.714
		298	0.912	0.228		
		303	0.675	0.99		
		308	0.575	1.416		
		313	0.551	1.551		
		318	0.517	1.751		

For PO_4^{3-} adsorption, across the entire experimental temperature range (20–45 °C), $\Delta H° < 0$ and $\Delta S° < 0$, corresponding to an exothermic process associated with a reduction in entropy. The capacity for adsorption dropped as the temperature rose, indicating a preference for lower temperatures[48–50]. The calculated $\Delta G°$ values were also positive in this case.

In general, the sign of $\Delta H°$ governs the temperature dependence of adsorption capacity: exothermic processes ($\Delta H° < 0$) are favored at lower temperatures, whereas endothermic processes ($\Delta H° > 0$) are enhanced at higher temperatures. Although all computed $\Delta G°$ values were positive—reflecting thermodynamic non-spontaneity under the defined standard conditions—the adsorption in actual non-standard systems is effectively driven by prevailing gradients such as concentration differences.

Repeated cycle experiments for NH_4^+ and PO_4^{3-}

To evaluate the reusability of BC5-500, it underwent five cycles of experimental testing, with results shown in Fig. 11. The adsorption of NH_4^+ exhibited a rapid decline in removal efficiency during the first three cycles. However, upon continuing the adsorption cycles, the removal efficiency remained largely stable. In summary, after five adsorption-desorption cycles, the NH_4^+ adsorption capacity of BC5-500 dropped by 4.2 mg·g^{-1}, with a corresponding 14% decrease in removal efficiency. For PO_4^{3-} adsorption, the initial adsorption capacity and removal efficiency were 145.29 mg·g^{-1} and 80.72%, respectively. After five cycles, the adsorption capacity and removal efficiency decreased to 93.84 mg·g^{-1} and 52.13%, respectively. Despite this reduction, the material still maintained a high adsorption capacity and a removal efficiency exceeding 50%, demonstrating that BC5-500 possesses good reusability and practicality.

Removal efficiency of NH_4^+ and PO_4^{3-} in actual swine wastewater

The swine wastewater was collected from a small-scale pig farm in Huangping County. After filtration, the wastewater had a pH of 7.48, with the following concentrations: NH_4^+ 84.00 mg·L^{-1}, PO_4^{3-} 14.54 mg·L^{-1}, Cu(II) 0.58 mg·L^{-1}, Cd(II) 0.15 mg·L^{-1}, tetracycline (TCH) 7.01 mg·L^{-1}, and oxytetracycline (OTC) 8.25 mg·L^{-1}. Then, 30 mL of wastewater were combined with a 0.05 g sample of BC5-500 and shaken for 120 min for NH_4^+ adsorption and for 360 min for PO_4^{3-} adsorption. Shaking was followed by filtering the liquid and measuring the remaining concentration.

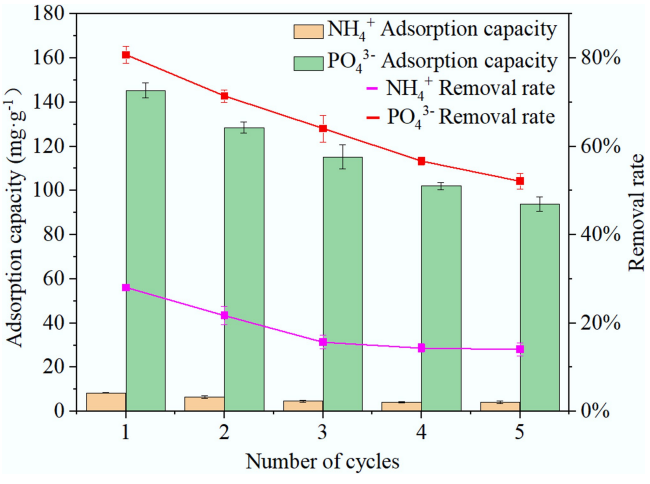

Fig. 11 Reusability of BC5-500 for the adsorption of NH_4^+ and PO_4^{3-} over five consecutive cycles.

As shown in Fig. 12, the adsorption capacities of BC5-500 for NH_4^+ and PO_4^{3-} were 6.93 and 8.52 mg·g^{-1}, respectively, with corresponding removal rates of 13.76% and 97.73%. The relatively low adsorption capacity for NH_4^+ in actual wastewater could be attributed to two main factors: first, the relatively low initial NH_4^+ concentration; second, the coexisting heavy metal ions and antibiotics likely compete with NH_4^+ for adsorption sites, thereby inhibiting its removal. The experimental results demonstrate that although BC5-500 shows limited NH_4^+ removal efficiency in complex aqueous matrices, its highly effective PO_4^{3-} removal capacity can still significantly mitigate the environmental risks associated with phosphorus-rich wastewater[51]. Thus, BC5-500 represents a promising material for practical wastewater treatment applications.

Reaction mechanism

The N_2 adsorption-desorption isotherm reveals that the modified material exhibits a Type IV isotherm and H1 hysteresis loop, indicating a mesoporous structure with relatively concentrated pore size distribution. The modified material exhibits increased SSA, pore volume, and average pore diameter. SEM analysis reveals a rougher surface with increased wrinkling and finer particles for BC5-500. This optimized porous structure enhances the adsorption of NH_4^+ and PO_4^{3-}. The adsorption mechanism of BC5-500 for NH_4^+ and PO_4^{3-} is illustrated in Fig. 13. XPS analysis indicates that the O–Ca structure content in BC5-500-N is lower than that in BC5-500, which is attributed to ion exchange between Ca^{2+} on BC5-500 and NH_4^+. FT-IR and XRD analyses indicate that the –OH groups on the BC5-500 surface react with phosphates in water to form $Ca_5(PO_4)_3(OH)$ precipitates, thereby adsorbing PO_4^{3-}. XPS analysis of BC5-500 reveals a 19.82% decrease in O–C=O content, indicating that O–C=O groups participated in the adsorption reaction with PO_4^{3-} and underwent ion exchange with $H_2PO_4^-$, HPO_4^{2-}, and PO_4^{3-}.

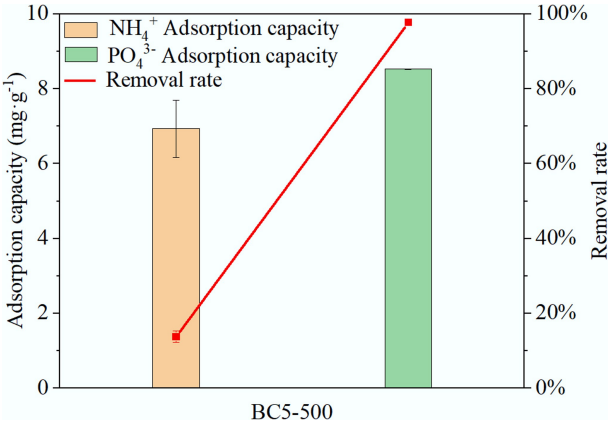

Fig. 12 Removal of NH_4^+ and PO_4^{3-} from actual swine wastewater by BC5-500.

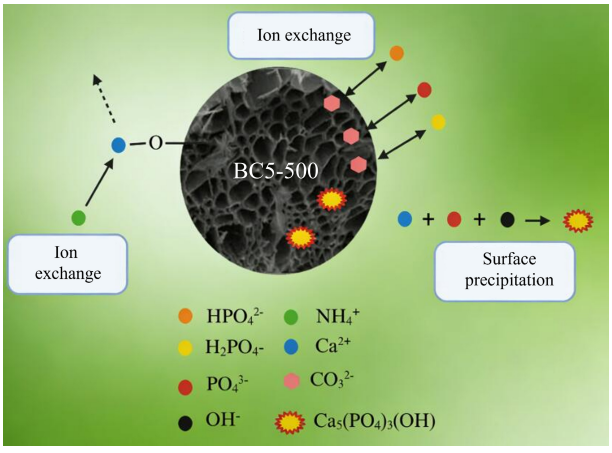

Fig. 13 Schematic diagram of the adsorption mechanism of NH_4^+ and PO_4^{3-} on BC5-500.

Conclusions

This study successfully synthesized a porous biochar (designated BC5-500) through $Ca(OH)_2$ modification of *Camellia oleifera* shells. For the simultaneous adsorption of NH_4^+ and PO_4^{3-}, the material displays excellent performance, reaching maximum capacities of 15.44 and 172.04 mg·g^{-1}. Alkaline conditions were favorable for NH_4^+ removal, whereas acidic conditions promoted PO_4^{3-} adsorption. The adsorption kinetics for both pollutants followed the pseudo-second-order model. Isotherm analysis indicated that NH_4^+ adsorption involved both monolayer and multilayer processes, while PO_4^{3-} adsorption was dominated by a multilayer mechanism. Mechanistic studies reveal that NH_4^+ removal occurs primarily via ion exchange, whereas PO_4^{3-} removal was mainly governed by Ca–P precipitation, with additional contributions from surface functional group interactions. BC5-500 retained stable adsorption performance over five consecutive reuse cycles. In actual swine wastewater, the PO_4^{3-} removal efficiency reached 97.73%, demonstrating its strong potential for practical application in the simultaneous recovery of nitrogen and phosphorus from wastewater.

Supplementary information

It accompanies this paper at: https://doi.org/10.48130/bchax-0026-0002.

Author contributions

The authors confirm contributions to the paper as follows: Min Chen: writing – original draft, methodology, validation; Xichang Wu: conceptualization, software, visualization; Yu Wang: software, visualization; Jie Wang: visualization, supervision; Chaochan Li: conceptualization; Tianhua Yu: software, formal analysis; Anping Wang: resources, conceptualization, supervision. All authors reviewed the results and approved the final version of the manuscript.

Data availability

The datasets generated during and/or analyzed during the current study are available from the corresponding author on reasonable request.

Funding

This work is supported by the project of the Guizhou Provincial Department of Science and Technology (Grant Nos Qiankehe Zhicheng [2023] 078, Qiankehe Jichu-ZK [2024] zhongdian 055, and Qiankehe Pingtai-KXJZ [2025] 023), and Projects of Forestry Research in Guizhou Province (Grant No. GUI[2022] TSLY07).

Declarations

Competing interests

The authors declare that they have no known competing financial interests or personal relationships that could have appeared to influence the work reported in this paper.

Author details

[1]Key Laboratory of Mountain Information System and Ecological Environment Protection, Guizhou Normal University, Guiyang 550025, China; [2]Qiandongnan Agriculture Science Institute, KaiLi 556099, China

References

[1] Hu Z, Li Z, Xu Y, He F, Zhang J, et al. 2025. MgFe-LDHs/*Vallisneria natans* combined system for simultaneous elimination of endogenous N and P pollution in eutrophic water: performance, synergetic mechanism, and metagenomics analysis. *Environmental Research* 279:121798

[2] Ke L, Liu X, Du B, Wang Y, Zheng Y, et al. 2022. Component analysis and risk assessment of biogas slurry from biogas plants. *Chinese Journal of Chemical Engineering* 44:182−191

[3] Ravindiran G, Rajamanickam S, Ramalingam M, Hayder G, Sathaiah BK, et al. 2024. Conversion of seaweed waste to biochar for the removal of heavy metal ions from aqueous solution: a sustainable method to address eutrophication problem in water bodies. *Environmental Research* 241:117551

[4] Lan Y, Gai S, Cheng K, Yang F. 2022. Advances in biomass thermochemical conversion on phosphorus recovery: water eutrophication prevention and remediation. *Environmental Science: Water Research & Technology* 8:1173−1187

[5] Peng L, Yin T, Song Z, Xiong S, Liu R, et al. 2025. Superior ammonia nitrogen adsorption capacity and reusability biochar microsphere applied in live fish transportation. *Chemical Engineering Journal* 514:163261

[6] Liu ZG, Min XB, Feng F, Tang X, Li WC, et al. 2021. Development and simulation of a struvite crystallization fluidized bed reactor with enhanced external recirculation for phosphorous and ammonium recovery. *Science of The Total Environment* 760:144311

[7] Guo J, Wen X, Yang J, Fan T. 2020. Removal of benzo(a)pyrene in polluted aqueous solution and soil using persulfate activated by corn straw biochar. *Journal of Environmental Management* 272:111058

[8] Wei B, Zhang D, Jeyakumar P, Trakal L, Wang H, et al. 2024. Iron-modified biochar effectively mitigates arsenic-cadmium pollution in paddy fields: a meta-analysis. *Journal of Hazardous Materials* 469:133866

[9] Wang CY, Wang Q, Zhou HD, Fang X, Zeng Q, et al. 2024. Adsorption of phosphate over a novel magnesium-loaded sludge-based biochar. *PLoS One* 19:e0301986

[10] Jiang YH, Li AY, Deng H, Ye CH, Wu YQ, et al. 2019. Characteristics of nitrogen and phosphorus adsorption by Mg-loaded biochar from different feedstocks. *Bioresource Technology* 276:183−189

[11] Li B, Jing F, Hu Z, Liu Y, Xiao B, et al. 2021. Simultaneous recovery of nitrogen and phosphorus from biogas slurry by Fe-modified biochar. *Journal of Saudi Chemical Society* 25:101213

[12] Palansooriya KN, Kim S, Igalavithana AD, Hashimoto Y, Choi YE, et al. 2021. Fe(III) loaded chitosan-biochar composite fibers for the removal of phosphate from water. *Journal of Hazardous Materials* 415:125464

[13] Cao H, Wu X, Syed-Hassan SSA, Zhang S, Mood SH, et al. 2020. Characteristics and mechanisms of phosphorous adsorption by rape straw-derived biochar functionalized with calcium from eggshell. *Bioresource Technology* 318:124063

[14] Wu L, Zhang S, Wang J, Ding X. 2020. Phosphorus retention using iron (II/III) modified biochar in saline-alkaline soils: adsorption, column and field tests. *Environmental Pollution* 261:114223

[15] Oginni O, Yakaboylu GA, Singh K, Sabolsky EM, Unal-Tosun G, et al. 2020. Phosphorus adsorption behaviors of MgO modified biochars derived from waste woody biomass resources. *Journal of Environmental Chemical Engineering* 8:103723

[16] Zeng S, Kan E. 2022. Sustainable use of Ca(OH)2 modified biochar for phosphorus recovery and tetracycline removal from water. *Science of The Total Environment* 839:156159

[17] Jiang D, Amano Y, Machida M. 2017. Removal and recovery of phosphate from water by calcium-silicate composites-novel adsorbents made from waste glass and shells. *Environmental Science and Pollution Research* 24:8210−8218

[18] Feng Y, Luo Y, He Q, Zhao D, Zhang K, et al. 2021. Performance and mechanism of a biochar-based Ca-La composite for the adsorption of phosphate from water. *Journal of Environmental Chemical Engineering* 9:105267

[19] Liu J, Wu L, Chen D, Li M, Wei C. 2017. Soil quality assessment of different *Camellia oleifera* stands in mid-subtropical China. *Applied Soil Ecology* 113:29−35

[20] Yang S, Li M, Wang Y, Liu X, Qing Y, et al. 2024. Industrial-scale manufacturing of particleboards using agricultural waste *Camellia oleifera* shells. *Construction and Building Materials* 424:135922

[21] Liu X, Wu Y, Gao Y, Jiang Z, Zhao Z, et al. 2024. Valorization of *Camellia oleifera* oil processing byproducts to value-added chemicals and biobased materials: a critical review. *Green Energy & Environment* 9:28−53

[22] Yu C. 2022. Recovery of NH_4^+–N and PO_4^{3-}–P from urine using sludge-derived biochar as a fertilizer: performance and mechanism. *RSC Advances* 12:4224−4233

[23] Huang Z, Chang B, Tang Y, Li Q, Zhang Z, et al. 2024. Co-adsorption performance and mechanism of ammonium and phosphate by iron-modified biochar in water. *Journal of Water Process Engineering* 67:106209

[24] Lee YE, Jeong Y, Shin DC, Ahn KH, Jung JH, et al. 2021. Fabrication of Mg-doped *Sargassum* biochar for phosphate and ammonium recovery. *Sustainability* 13:12752

[25] He Q, Li X, Ren Y. 2022. Analysis of the simultaneous adsorption mechanism of ammonium and phosphate on magnesium-modified biochar and the slow release effect of fertiliser. *Biochar* 4:25

[26] Lv C, Liu P, Cheng S. 2024. Preparation of biochar from pyrolysis of soybean straw at different pyrolysis temperature for cadmium removal from wastewater and pyrolysis gas investigation. *Arabian Journal of Chemistry* 17:105946

[27] Cantrell KB, Hunt PG, Uchimiya M, Novak JM, Ro KS. 2012. Impact of pyrolysis temperature and manure source on physicochemical characteristics of biochar. *Bioresource Technology* 107:419−428

[28] Xu D, Ni X, Kang J, He B, Zuo Y, et al. 2024. Mechanisms of cadmium adsorption by ramie nano-biochar with different aged treatments. *Applied Soil Ecology* 193:105175

[29] Gong H, Zhang X, Wang G, Liu Y, Li Y, et al. 2020. Dodecahedron ZIF-67 anchoring ZnCdS particles for photocatalytic hydrogen evolution. *Molecular Catalysis* 485:110832

[30] Jiang Y, Xing Y, Liu S, Tan S, Huang Q, et al. 2023. A longer biodegradation process enhances the cadmium adsorption of the biochar derived from a manure mix. *Biomass and Bioenergy* 173:106787

[31] Pan F, Wei H, Huang Y, Song J, Gao M, et al. 2024. Phosphorus adsorption by calcium chloride-modified buckwheat hulls biochar and the potential application as a fertilizer. *Journal of Cleaner Production* 444:141233

[32] Wang K, Peng N, Zhang D, Zhou H, Gu J, et al. 2023. Efficient removal of methylene blue using $Ca(OH)_2$ modified biochar derived from rice straw. *Environmental Technology & Innovation* 31:103145

[33] Liao Y, Chen S, Zheng Q, Huang B, Zhang J, et al. 2022. Removal and recovery of phosphorus from solution by bifunctional biochar. *Inorganic Chemistry Communications* 139:109341

[34] Liu X, Shen F, Qi X. 2019. Adsorption recovery of phosphate from aqueous solution by CaO-biochar composites prepared from eggshell and rice straw. *Science of The Total Environment* 666:694−702

[35] Dermawan D, Satriavi AD, Nurhidayati DI, Firnandi R, Mayangsari NE, et al. 2025. Composite adsorbent from sugarcane (*Saccharum officinarum*) bagasse biochar generated from atmospheric pressure microwave plasma pyrolysis process and nano zero valent iron (nZVI) for rapid and highly efficient Cr(VI) adsorption. *Case Studies in Chemical and Environmental Engineering* 11:101123

[36] Deng W, Zhang D, Zheng X, Ye X, Niu X, et al. 2021. Adsorption recovery of phosphate from waste streams by Ca/Mg-biochar synthesis from marble waste, calcium-rich sepiolite and bagasse. *Journal of Cleaner Production* 288:125638

[37] Wang Z, Wang F, Cao J, Wang J. 2010. Pyrolysis of pine wood in a slowly heating fixed-bed reactor: potassium carbonate versus calcium hydroxide as a catalyst. *Fuel Processing Technology* 91:942−950

[38] Li H, Wang Y, Zhao Y, Wang L, Feng J, et al. 2023. Efficient simultaneous phosphate and ammonia adsorption using magnesium-modified biochar beads and their recovery performance. *Journal of Environmental Chemical Engineering* 11:110875

[39] Chang H, Yang XY, Liang D, Chen ZQ, Liu X. 2024. Enhanced removal of ammonium nitrogen from aqueous solutions using a novel biochar derived from millet shells through both static adsorption and dynamic column experiments. *Journal of Water Process Engineering* 58:104848

[40] Wang S, Ai S, Nzediegwu C, Kwak JH, Islam MS, et al. 2020. Carboxyl and hydroxyl groups enhance ammonium adsorption capacity of iron (III) chloride and hydrochloric acid modified biochars. *Bioresource Technology* 309:123390

[41] Grimm A, dos Reis GS, Khokarale SG, Ekman S, Lima EC, et al. 2023. Shiitake spent mushroom substrate as a sustainable feedstock for developing highly efficient nitrogen-doped biochars for treatment of dye-contaminated water. *Journal of Water Process Engineering* 56:104435

[42] Tan M, Zhao Y, Quan B, Wu Q, Chi D, et al. 2024. Synergistic removal of ammonium and phosphate using ultrasonic Mg-based biochar composite: mechanism, behavior and green recycling. *Journal of Environmental Chemical Engineering* 12:111995

[43] Reguyal F, Sarmah AK, Gao W. 2017. Synthesis of magnetic biochar from pine sawdust via oxidative hydrolysis of $FeCl_2$ for the removal sulfamethoxazole from aqueous solution. *Journal of Hazardous Materials* 321:868−878

[44] Feng Q, Chen M, Wu P, Zhang X, Wang S, et al. 2022. Simultaneous reclaiming phosphate and ammonium from aqueous solutions by calcium alginate-biochar composite: sorption performance and governing mechanisms. *Chemical Engineering Journal* 429:132166

[45] Zhuo SN, Dai TC, Ren HY, Liu BF. 2022. Simultaneous adsorption of phosphate and tetracycline by calcium modified corn stover biochar: performance and mechanism. *Bioresource Technology* 359:127477

[46] Xiong S, Gong D, Deng Y, Tang R, Li L, et al. 2021. Facile one-pot magnetic modification of *Enteromorpha prolifera* derived biochar: increased pore accessibility and Fe-loading enhances the removal of butachlor. *Bioresource Technology* 337:125407

[47] Fu L, Li J, Wang G, Luan Y, Dai W. 2021. Adsorption behavior of organic pollutants on microplastics. *Ecotoxicology and Environmental Safety* 217:112207

[48] Al-Ghouti MA, Da'ana DA. 2020. Guidelines for the use and interpretation of adsorption isotherm models: a review. *Journal of Hazardous Materials* 393:122383

[49] Biswas B, Adhikari S, Jahromi H, Ammar M, Baltrusaitis J, et al. 2024. Magnesium doped biochar for simultaneous adsorption of phosphate and nitrogen ions from aqueous solution. *Chemosphere* 358:142130

[50] He Y, Zhang L, An X, Wan G, Zhu W, et al. 2019. Enhanced fluoride removal from water by rare earth (La and Ce) modified alumina: adsorption isotherms, kinetics, thermodynamics and mechanism. *Science of The Total Environment* 688:184−198

[51] Wang Q, Wang CY, Zhou HD, Xue DX, Xiong XL, et al. 2024. Simultaneous adsorption of ammonia nitrogen and phosphate on electro-assisted magnesium/aluminum-loaded sludge-based biochar and its utilization as a plant fertilizer. *PLoS One* 19:e0311430